A&A 634, A88 (2020)
https://doi.org/10.1051/0004-6361/201937124

Astronomy & Astrophysics

Mass constraints for 15 protoplanetary discs from HD 1–0

M. Kama[1,2], L. Trapman[3], D. Fedele[4], S. Bruderer[5], M. R. Hogerheijde[2,6], A. Miotello[7], E. F. van Dishoeck[2,5], C. Clarke[1], and E. A. Bergin[8]

[1] Institute of Astronomy, University of Cambridge, Madingley Road, Cambridge CB3 0HA, UK
e-mail: mkama@ast.cam.ac.uk
[2] Tartu Observatory, Observatooriumi 1, Tõravere 61602, Tartu, Estonia
e-mail: mihkel.kama@ut.ee
[3] Leiden Observatory, Leiden University, Niels Bohrweg 2, 2333 CA Leiden, The Netherlands
[4] INAF – Osservatorio Astrofisico di Arcetri, Largo E. Fermi 5, 50125 Firenze, Italy
[5] Max-Planck-institute für extraterrestrische Physic, Giessenbachstraße, 85748 Garching bei München, Germany
[6] Anton Pannekoek Institute for Astronomy, University of Amsterdam, Science Park 904, 1090 GE Amsterdam, The Netherlands
[7] European Southern Observatory, Karl-Schwarzschild-Str. 2, 85748 Garching bei München, Germany
[8] Department of Astronomy, University of Michigan, 1085 S. University Ave, Ann Arbor, MI 48109, USA

Received 16 November 2019 / Accepted 22 December 2019

ABSTRACT

Context. Hydrogen deuteride (HD) rotational line emission can provide reliable protoplanetary disc gas mass measurements, but this molecule is difficult to observe and detections have been limited to three T Tauri discs. No new data have been available since the *Herschel* Space Observatory mission ended in 2013.

Aims. We set out to obtain new disc gas mass constraints by analysing upper limits on HD 1–0 emission in *Herschel*/PACS archival data from the DIGIT key programme.

Methods. With a focus on the Herbig Ae/Be discs, whose stars are more luminous than T Tauris, we determined upper limits for HD in data previously analysed for its line detections. We studied the significance of these limits with a grid of models run with the DALI physical-chemical code, customised to include deuterium chemistry.

Results. Nearly all the discs are constrained to $M_{\rm gas} \leq 0.1\,M_{\odot}$, ruling out global gravitational instability. A strong constraint is obtained for the HD 163296 disc mass, $M_{\rm gas} \leq 0.067\,M_{\odot}$, implying $\Delta_{\rm g/d} \leq 100$. This HD-based mass limit is towards the low end of CO-based mass estimates for the disc, highlighting the large uncertainty in using only CO and suggesting that gas-phase CO depletion in HD 163296 is at most a factor of a few. The $M_{\rm gas}$ limits for HD 163296 and HD 100546, both bright discs with massive candidate protoplanetary systems, suggest disc-to-planet mass conversion efficiencies of $M_{\rm p}/(M_{\rm gas}+M_{\rm p}) \approx 10$–40% for present-day values. Near-future observations with SOFIA/HIRMES will be able to detect HD in the brightest Herbig Ae/Be discs within 150 pc with ≈ 10 h integration time.

Key words. planets and satellites: formation – protoplanetary discs – circumstellar matter – planets and satellites: gaseous planets

1. Introduction

The elusive total gas mass of a protoplanetary disc is relevant for planet formation, dust dynamics, and for testing disc evolution models. As a result of difficulties in observing H_2, $M_{\rm gas}$ has been robustly measured in only three cases (Bergin et al. 2013; McClure et al. 2016). In this work, we use *Herschel* archival data to constrain $M_{\rm gas}$ in a sample of 15 Herbig Ae/Be discs, and we determine the mass of HD 163296 to within a factor of a few.

The gas mass is dominated by H_2, which has a large energy spacing between its lowest rotational levels (*para*-H_2 $J = 2$–0, $\Delta E = 512$ K) and lacks a dipole moment. As such, H_2 is not emissive at the 10–100 K temperatures typical for discs. Dust continuum emission at millimetre wavelengths is often used to estimate $M_{\rm gas}$. Gas and dust are linked through a mass ratio, canonically $\Delta_{\rm g/d} = 100$ for solar-composition material below $\sim 10^3$ K (e.g. Lodders 2003). While dust emission is easy to detect, the different dust and gas evolution as well as uncertain opacity values limit its reliability in measuring $M_{\rm gas}$. The most precise $M_{\rm gas}$ measurements to date are from hydrogen deuteride (HD) rotational lines. The relative abundance of this deuterated isotopologue of H_2 is set by the local absolute atomic ratio, $D/H = (2.0 \pm 0.1) \times 10^{-5}$ (Prodanović et al. 2010), and is minimally affected by disc chemistry (Trapman et al. 2017). As the $J = 1$ rotational level is at $E/k_B = 128.5$ K, HD emits from warm gas ($T_{\rm gas} \approx 30$–50 K; Bergin et al. 2013; Trapman et al. 2017). This is sufficient to constrain the total $M_{\rm gas}$, especially if the temperature structure is constrained via other observables. The HD $J = 1$–0 line at 112 μm is however impossible to observe from the ground owing to atmospheric absorption and requires air- or space-borne telescopes.

After the pioneering HD 1–0 detection in TW Hya (Bergin et al. 2013; Trapman et al. 2017), facilitated by the PACS spectrometer (Poglitsch et al. 2010) on the *Herschel* Space Observatory (Pilbratt et al. 2010), further detections were only made in DM Tau and GM Aur (McClure et al. 2016) before the instrument expired. The masses of these T Tauri discs are $M_{\rm gas} = (6$–$9) \times 10^{-3}$, $(1$–$4.7) \times 10^{-2}$, and $(2.5$–$20.4) \times 10^{-2}\,M_{\odot}$, respectively. An upper limit $M_{\rm gas} \leq 8 \times 10^{-2}\,M_{\odot}$ was obtained for the Herbig Ae/Be system HD 100546 (Kama et al. 2016, revised down from the published value because of a mistake in the D/H ratio).

Table 1. HD line flux upper limits (3σ) for the sample.

Name	$L_\star$ ($L_\odot$)	$T_{\rm eff}$ (K)	d (pc)	HD 112 μm $\left(10^{-17}\,\frac{\rm W}{\rm m^2}\right)$	HD 56 μm $\left(10^{-17}\,\frac{\rm W}{\rm m^2}\right)$	$F_{\rm 1.3mm}$ (mJy)	Meeus group
HD 104237	26[F15]	8000[F15]	108[GDR2]	≤0.9	≤2.4	92 ± 19[M14]	IIa
HD 144668	58[F15]	8500[F15]	161[GDR2]	≤0.8	≤7.8	20 ± 16[M14]	IIa
HD 163296	31[F12]	9200[F12]	101[GDR2]	≤0.6	≤3.0	743 ± 15[M14]	IIa
HD 31293	59[F15]	9800[F12]	139[F12]	≤4.2	≤22.4	136 ± 15[M14]	Ia
HD 36112	22[M14]	8190[F12]	160[GDR2]	≤0.6	≤7.6	72 ± 13[M14]	Ia
HD 38120	123[S13]	10471[S13]	406[GDR2]	≤0.9	≤5.6	–	Ia
HD 100546	36[K16b]	10390[K16b]	110[GDR2]	≤2.7	≤16.0	465 ± 20[M14]	Ia
HD 139614	6.6[F15]	7750[F15]	135[GDR2]	≤1.2	≤8.5	242 ± 15[M14]	Ia
HD 142527	7.9[F15]	6500[F15]	157[GDR2]	≤4.0	≤13.0	1190 ± 33[M14]	Ia
HD 179218	110[F12]	9640[F12]	266[GDR2]	≤1.1	≤7.0	71 ± 7[M14]	Ia
HD 97048	33[F15]	10500[F15]	171[F15]	≤2.4	≤2.4	454 ± 34[M14]	Ib
HD 100453	8.5[F15]	7250[F15]	104[GDR2]	≤1.3	≤5.5	200 ± 21[M14]	Ib
HD 135344B	7.1[F15]	6375[F15]	136[GDR2]	≤0.6	≤8.2	142 ± 19[M14]	Ib
HD 169142	10[F12]	7500[F12]	114[GDR2]	≤2.4	≤13.5	197 ± 15[M14]	Ib
Oph IRS 48[(a)]	14.3[S13]	9000[S13]	134[GDR2]	≤1.2	≤8.3	60 ± 10[M14]	Ib

Notes. [(a)]WLY 2-48.

References. F12 – Folsom et al. (2012); S13 – Salyk et al. (2013); M14 – Maaskant et al. (2014) and references therein; F15 – Fairlamb et al. (2015); K16b – Kama et al. (2016); GDR2 – Brown et al. (2018).

In this work, we use the 2D physical-chemical code `DALI` (Bruderer et al. 2012; Bruderer 2013) to constrain $M_{\rm gas}$ in 15 discs by analysing *Herschel* Space Observatory archival data covering the HD 1–0 and 2–1 lines. The data and models are discussed in Sects. 2 and 3, respectively. In Sect. 4, we explore the disc mass constraints, with a focus on HD 163296, and discuss the potential for gravitational instability. In Sect. 5, we compare the mass of discs, stars, and planetary systems for stars over 1.4 $M_\odot$. We also discuss future observations of HD with SOFIA/HIRMES (Richards et al. 2018) and SPICA/SAFARI (Nakagawa et al. 2014; Audley et al. 2018).

2. Observations and sample

We use archival data from the *Herschel* Space Observatory (Pilbratt et al. 2010) key programme DIGIT (PI: N.J. Evans), which targeted 30 protoplanetary discs with the PACS (Poglitsch et al. 2010) instrument at 50–210 μm. Detected gaseous species in this data are presented in Fedele et al. (2013) and Meeus et al. (2013). We analyse upper limits on HD J = 1–0 and 2–1 lines at 112 and 56 μm for the 15 Herbig Ae/Be discs in the sample. Because of the intrinsically higher luminosity of their host stars (~10–100 $L_\odot$), these discs are warmer and brighter in continuum and line emission than those around T Tauri stars. This enables tighter constraints for discs at equivalent distance.

We selected discs around stars of spectral type mid-F to late-B, including well-known targets such as HD 100546 and HD 163296. HD 50138 was excluded as it is likely an evolved star (Ellerbroek et al. 2015), and HD 35187 was excluded because it is a binary of two intermediate-mass stars and not directly comparable to our model grid. The data are spectrally unresolved, with $\delta v \approx 100$ km s^{-1} ($\lambda/\delta\lambda$ = 3000) at the shortest wavelengths (51 μm), while expected linewidths are ≤10 km s^{-1}. Exposure times ranged from 4356 to 8884 s. The system parameters and 3σ line flux upper limits are given in Table 1.

We obtained flux limits for the HD transitions from the 1σ noise reported for the nearest lines of other molecules from Fedele et al. (2013): OH $^2\Pi_{1/2}$ $J = 9/2^-$–$7/2^+$ at 55.89 μm for the 56 μm line and OH $^2\Pi_{3/2}$ $J = 5/2^-$–$3/2^+$ at 119.23 μm for the 112 μm line. With a typical 1σ uncertainty of 5×10^{-18} W m^{-2} at 112 μm and 2×10^{-17} W m^{-2} at 56 μm, neither of the HD lines is detected in the targets, individually or stacked. For comparison, the HD 1–0 detections in Bergin et al. (2013) and McClure et al. (2016) have respective uncertainties of roughly 7×10^{-19} W m^{-2} and 5×10^{-19} W m^{-2}, which illustrates the difference between those targeted, deep integrations and the survey-type observations analysed in this work.

The discs fall into two categories: cold (flat, group II in the Meeus classification, Meeus et al. 2001) and warm (flaring, group I). This characterises the shape of the radial optically thick surface, where starlight is effectively absorbed. Starlight impinges at a shallow angle on flat discs, and heating is inefficient compared to that above the same mid-plane location in a flaring disc. In addition, among the Herbig Ae/Be systems flaring, group I discs have resolved cavities or gaps 10–100 au scales in their millimetre dust emission (Maaskant et al. 2013; Kama et al. 2015).

3. Modelling

3.1. DALI

To determine the behaviour of the HD 1–0 line and 1.3 mm continuum flux as a function of disc structure parameters, we ran a grid of models with the 2D physical-chemical disc code `DALI` (Bruderer et al. 2012; Bruderer 2013). The surface density is parametrised following the viscous accretion disc formalism (Lynden-Bell & Pringle 1974; Hartmann et al. 1998):

$$\Sigma_{\rm gas} = \Sigma_{\rm c}\left(\frac{R}{R_{\rm c}}\right)^{\gamma}\exp\left[-\left(\frac{R}{R_{\rm c}}\right)^{2-\gamma}\right], \quad (1)$$

where $\Sigma_{\rm c}$ is the surface density at the characteristic radius $R_{\rm c}$ and γ the power-law index, which is generally 1. Assuming an isothermal structure in hydrostatic equilibrium, the vertical structure is given by a Gaussian density distribution (Kenyon & Hartmann 1987):

$$\rho_{\rm gas}(R,z) = \frac{\Sigma_{\rm gas}(R)}{\sqrt{2\pi}Rh}\exp\left[-\frac{1}{2}\left(\frac{z}{Rh}\right)^2\right]. \quad (2)$$

In this equation $h = h_c(R/R_c)^{\psi}$, ψ is the flaring index, and h_c is the disc opening angle at R_c.

A population of small grains (0.005–1 μm), which have a mass fraction $f_{\rm small}$, follows the gas density distribution given in Eq. (2). A second population, consisting of large grains (1 μm–1 mm), has a mass fraction $f_{\rm large}$. The scale height of this second population is χh, where $\chi \in (0, 1)$ is the settling parameter.

For the dust opacities of both small and large grain populations we assume a standard interstellar composition following Weingartner & Draine (2001), in line with Bruderer (2013). The absorption coefficient for the small (large) grains is 29.9 $\rm cm^2\,g^{-1}$ (30.0 $\rm cm^2\,g^{-1}$) at 112 μm and 154 $\rm cm^2\,g^{-1}$ (46.3 $\rm cm^2\,g^{-1}$) at 56 μm.

First, the radiation field and dust temperature are determined from Monte Carlo radiative transfer. Next, the gas temperature (heating-cooling balance) and chemical composition (steady-state) are solved for iteratively. Raytracing then yields simulated line and continuum observations.

HD chemical network versus fixed abundance. The HD abundance (HD/H_2) can be prescribed as a constant or obtained from solving a chemical reaction network. In the parametric approach, the HD abundance is determined by the local D/H ratio, which for the local interstellar medium (ISM; within ≈2 kpc) is measured to be $(D/H)_{\rm ISM} = (2.0 \pm 0.1) \times 10^{-5}$ (Prodanović et al. 2010). Assuming all deuterium is in HD, this gives $HD/H_2 = 4 \times 10^{-5}$.

A more refined approach is to calculate the HD abundance using a reaction network which includes deuterium. Trapman et al. (2017) extends the standard DALI chemical network (originally based on the UMIST06 database Woodall et al. 2007) to include the species HD, D, HD^+, and D^+. These authors include HD formation on dust and ion-exchange reactions in addition to HD self-shielding. The details of the implementation are described in Sect. 2.3 of Trapman et al. (2017).

Using the chemical network approach, we find that all of the available deuterium is locked up in HD for the vast majority of the disc, and the parametric abundance of $HD/H_2 = 4 \times 10^{-5}$ is appropriate to use. The network produces less HD in only two regions: the uppermost layers of the disc where HD is photodissociated and in a thin intermediate layer, where the HD abundance is decreased by a factor of ∼2. Tests determined that neither of these significantly affects the disc-integrated HD line flux. Given the very close match between the two approaches, we opt for simplicity and fix the HD/H_2 ratio at 4×10^{-5}.

Part of our analysis below involves modelling CO rotational lines. Owing to processes such as chemical conversion and freeze-out, the gas-phase total abundance of C and O nuclei can be more than a factor of ten below nominal (e.g. Favre et al. 2013; Kama et al. 2016), which makes CO-based mass estimates highly uncertain. We refer to the reduction of gas-phase C and O nuclei below their total values with the term depletion, and the phenomenon can be included in our modelling as a reduction of the total amount of volatile C or O input into a given DALI model. This is relevant for Sect. 4.3, in particular.

Table 2. DALI model grid parameters.

Parameter	Range
Chemistry	
Chemical age	1 Myr
HD/H_2	4×10^{-5}
Physical structure	
γ	1.0
ψ	[0.0, 0.3]
h_c	[0.05, 0.15] rad
R_c	[50, 150] au
$M_{\rm gas}$	$[10^{-3}, 10^{-2}, 10^{-1}]\ M_\odot$
Dust properties	
$\Delta_{\rm g/d}$	[10, 50, 100, 300]
$f_{\rm large}$	[0.8, 0.95]
χ	[0.2, 0.5]
$f_{\rm PAH}$	0.001
Stellar properties[1]	
$T_{\rm eff}$	10 390 K
L_X	8×10^{28} erg $\rm s^{-1}$
T_X	7×10^{7} K
L_*	[10, 50, 115] $L_\odot$
$\zeta_{\rm cr}$	$10^{-17}\ \rm s^{-1}$
Observational geometry	
i	60°
d	150 pc

Notes. Standard DALI parameter names as in Bruderer et al. (2012). Deuterium abundance from Prodanović et al. (2010). [(1)]HD 100546 (Bruderer et al. 2012). The model grid can be accessed at https://zenodo.org/record/3625990.

3.2. Model grid

To investigate the range of disc properties constrained by the *Herschel* upper limits on the HD 1–0 line, we ran a grid of Herbig Ae/Be disc models covering a wide range of parameters, summarised in Table 2. The disc gas masses are $M_{\rm gas} = 10^{-3}$, 10^{-2}, and $10^{-1}\ M_\odot$. Dust mass is defined by the gas-to-dust mass ratio that has values $\Delta_{\rm g/d} = 10$, 50, 100, and 300 and ranges from $M_{\rm dust} = 3 \times 10^{-6}$ to $10^{-2}\ M_\odot$. The shape of the stellar spectrum, including UV excess, is based on HD 100564 from Bruderer et al. (2012). The spectrum is scaled to the total stellar luminosity, $L_\star \in [10, 50, 115]\ L_\odot$. This covers the sources in our sample, as given in Table 1. In total we ran 2304 models; parameters are given in Table 2. Our fiducial model has $h_c = 0.15$, $R_c = 50$ au, $\Delta_{\rm gd} = 100$, $f_{\rm large} = 0.95$, $\chi = 0.2$, and $L_\star = 10\ L_\odot$.

Figure 1 shows the HD 1–0 emitting regions and disc mass outline for models representing extremes in flaring ($\Psi = 0.0$ and $h_c = 0.05$ for flat, and $\Psi = 0.3$ and $h_c = 0.15$ for flared), radial extent ($R_c = 50$ and 125 au), and total disc mass. From the figure it is clear that the flared disc ($\psi = 0.3, h_c = 0.15$), shown in red, has a much large emitting region than the flat disc ($\Psi = 0.0, h_c = 0.05$), shown in blue. In both cases the HD 1–0 emission originates from the warm layer above the midplane.

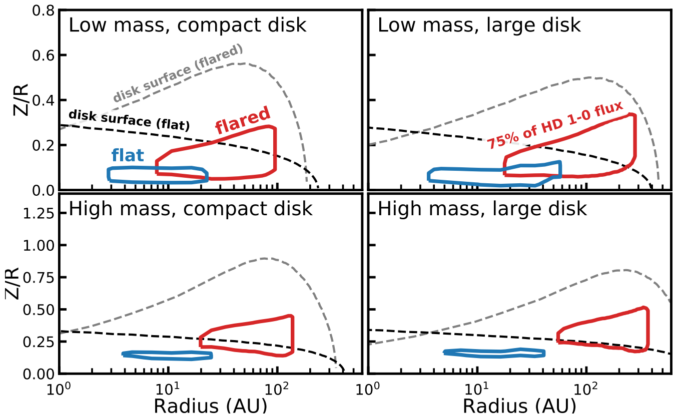

Fig. 1. HD1–0 line emitting regions in our flat/cold (blue) and flared/warm (red) disc models. Solid contours contain the middle 75% of cumulative line emission. Dashed lines indicate gas number density iso-contours for $n_{\rm gas} = 10^6$ cm^{-3}, acting as a disc outline.

Table 3. Adopted model for HD 163296.

Parameter	Value
γ	0.9
ψ	0.05
h_c	0.075
R_c	125 au
Σ_c $R_{\rm cav}$	0.41 au
$M_{\rm gas}$	6.7×10^{-2} $M_\odot$
$M_{\rm dust}$	6.6×10^{-4} $M_\odot$
$\Delta_{g/d}$	100
$f_{\rm large}$	0.9
χ	0.2
L_* ($L_\odot$)	37.7
i (°)	45
d (pc)	101 pc

4. Results

In Fig. 2, we show the HD $J = 1$–0 flux as a function of $M_{\rm gas}$ and 1.3 mm continuum flux. The warm, flaring, group I discs and cold, flat, group II discs are highlighted separately for clarity.

4.1. Parameter dependences in the grid

Dependences of the HD 1–0 line and 1.3 mm continuum flux on the main model parameters are shown in Fig. 3. The HD line flux depends linearly on $M_{\rm gas}$, which has only a marginal effect on the dust emission. For a fixed $M_{\rm gas}$, a 1 dex increase in $M_{\rm dust}$ leads to a factor 6.7 lower HD and 2.5 higher continuum flux. The flaring structure of the disc has the largest influence, as the HD line flux increases by a factor of 26 when the flaring parameter Ψ goes from 0 (height is linear with radius, inefficient heating) to 0.3 (very flared and efficiently heated). The Meeus group corresponds to the flaring structure (group I discs are flared, II flat).

A near-linear dependence of HD line flux on $M_{\rm gas}$ arises because the HD line emission in the models is vertically limited by the dust optical depth τ at 112 μm out to ≈100 au radii, beyond which the surface density drops rapidly. Thus the HD contribution from the gas above and radially outside the dust scales linearly with the total gas mass. Dust emission, to first order, is optically thin at 1.3 mm, and thus scales linearly with the total dust mass. Again because the dust optical depth dominates at the 112 μm wavelength of HD 1–0, increasing the dust mass in a given column lifts the vertical $\tau(112\,\mu{\rm m}) = 1$ surface, hiding a larger fraction of the HD molecules.

4.2. Constraints on M_{gas} across the sample

A comparison of the HD upper limits from *Herschel* with our `DALI` model grid (Figs. 2 and 4) places an upper limit of approximately $M_{\rm gas} \leq 0.1\,M_\odot$ for the discs in our sample. Among the flared, group I discs (Fig. 2, upper row), we find $M_{\rm gas} < 0.02$–$0.03\,M_\odot$ for IRS 48, HD 36112, HD 100453, and HD 135344B, while among the flat, group II discs HD 163296 has a limit at $<0.1\,M_\odot$.

Source-specific models can tighten the mass limit for individual discs. We ran a small grid of models for HD 163296, in which we have a strong HD upper limit and a wide comparison range of indirect gas mass estimates from the literature based on various isotopologues of CO.

4.3. HD 163296

We constrain the gas mass in the HD 163296 disc to $M_{\rm gas} \leq 0.067\,M_\odot$ (Fig. 5). Given that the disc-integrated dust mass in our model is $6.7\times10^{-4}\,M_\odot$, this constrains the gas-to-dust ratio to $\Delta_{g/d} \leq 100$ and has implications for the gas-phase volatile abundances, which we discuss below. This source-specific model matches the continuum spectral energy distribution, ^{12}CO rotational ladder and isotopologue lines, and several other key volatile species. The full details of this modelling are outside the scope of this paper and will be published separately; below we focus on the main outcomes of the continuum, CO, and HD modelling.

HD 163296 is one of the largest known discs with a CO J = 3–2 gas emission radius of 540 au (Rosenfeld et al. 2013). Fitting of CO and 850 μm continuum emission, observed by ALMA, with a tapered surface density power law yielded γ = 0.9 and R_c = 125 au (Tilling et al. 2012; de Gregorio-Monsalvo et al. 2013). We model HD 163296 with the stellar spectrum from the ProDiMo project (Woitke et al. 2019), fixing the shape of the dust surface density profile to the above parameters and varying the gas mass. To satisfy the radial profile of CO 3–2 emission simultenaously with the spectral energy distribution, we find the density profile flaring index in Eq. (2) is around ψ = 0.05, consistent with the range 0.019–0.066 found by Tilling et al. (2012). The morpology of the ^{12}CO 3–2 channel maps, in which both the near and far side of the disc can be seen, suggest HD 163296 is more flared ($\psi \approx 0.12$, de Gregorio-Monsalvo et al. 2013) than our model (ψ = 0.05). However, these two ψ-s differ in physical meaning: the CO-based ψ measures the observed shape of the CO-emitting surface, while the disc structure parameter ψ characterises the shape of the total gas mass distribution (see Eq. (2)).

Our model, which hits the HD upper limit, reproduces the observed dust emission across the far-infrared and submillimetre wavelengths as well as various spatially resolved and unresolved emission lines of ^{12}CO and its isotopologues, and has a gas-to-dust ratio $\Delta_{g/d}$ = 100.

Most previous estimates of the HD 163296 gas mass relied on low-J emission lines of CO isotopologues, and used a

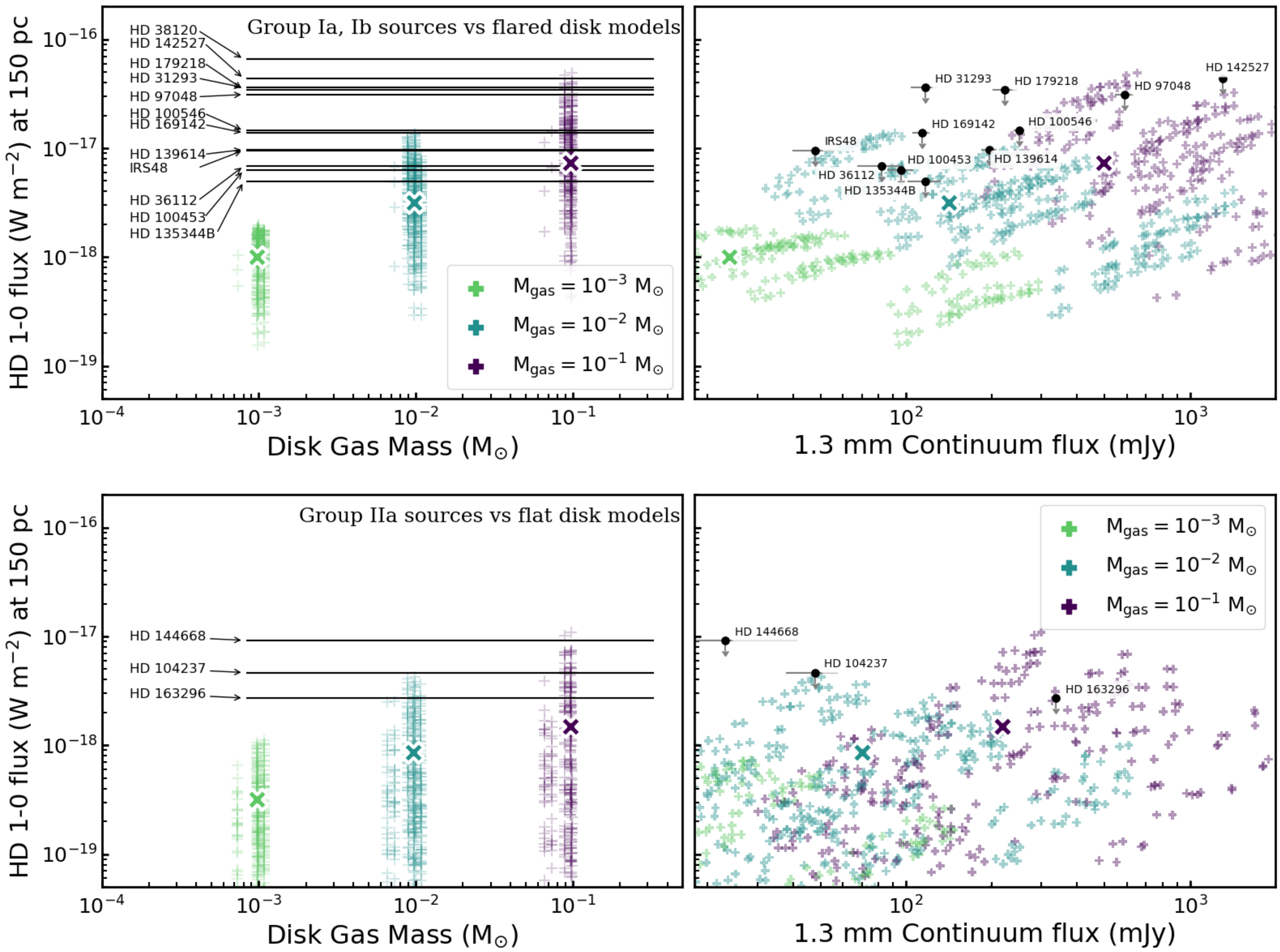

Fig. 2. Distance-normalised 3σ upper limits on HD 112 μm line flux for the disc sample (black lines and circles) compared with our grid of DALI disc models (coloured crosses). Highlighted crosses show the HD 112 μm line flux of our fiducial model. The top panels show the group I sources compared to models with flaring angle $\psi = 0.3$. The bottom panels show the group II sources compared to models with $\psi = 0.0$. *Left*: models are separated based on gas mass. *Right*: HD 1–0 upper limits set against 1.3 mm continuum fluxes for both observations and models.

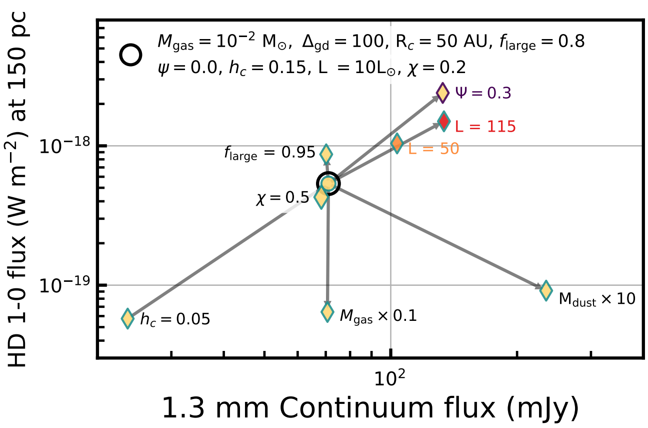

Fig. 3. HD 1–0 line and dust continuum flux dependences on disc and stellar parameters.

range of modelling approaches from generic model grids to tailored modelling with physical-chemical codes. Those $M_{\rm gas}$ estimates range from 8×10^{-3} to $5.8\times10^{-1}\,M_\odot$ (Isella et al. 2007; Williams & Best 2014; Boneberg et al. 2016; Miotello et al. 2016; Williams & McPartland 2016; Powell et al. 2019; Woitke et al. 2019; Booth et al. 2019). The mass obtained from the most optically thin isotopologue among these, $^{13}C^{17}O$, was $2.1\times10^{-1}\,M_\odot$ (Booth et al. 2019).

Above, we assumed an undepleted solar abundance for elemental gas-phase carbon and oxygen. Our model matching the HD upper limit overproduces the low-J line fluxes of CO isotopologues by a factor of a few. Since the rarer isotopologues are progressively more optically thin, we can reproduce their line fluxes by decreasing the gas-phase elemental carbon and oxygen abundance proportionately to the flux mismatch. Since the millimetre-wave dust emission and HD upper limit constrain the gas-to-dust mass ratio to be $\leq$100, we can combine the above considerations to arrive at the following three distinct hypotheses for HD 163296.

1. $M_{\rm gas}$ is just sufficiently below our upper limit of $6.7\times10^{-2}\,M_\odot$ for HD not to be detected. If so, then as the dust mass is fixed, it follows from our models that $\Delta_{\rm g/d} = 100$ and that total gas-phase elemental C and O are depleted by up to a factor of a few.
2. $M_{\rm gas}$ is a factor of a few below our HD limit, and the total gas-phase elemental C and O abundances are not depleted with respect to their interstellar values. If so, the implication

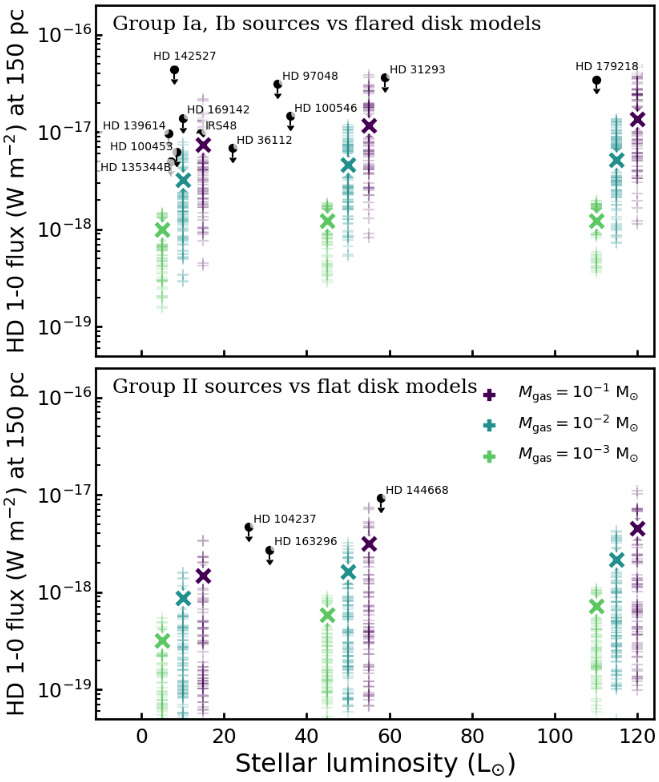

Fig. 4. HD 1–0 line flux vs. stellar luminosity. Observed stellar luminosities taken from Table 1. Model stellar luminosities are given a small offset for clarity. Highlighted crosses show our fiducial model ($h_c = 0.15$, $R_c = 50$ au, $\Delta_{gd} = 100$, $f_{large} = 0.95$, $\chi = 0.2$).

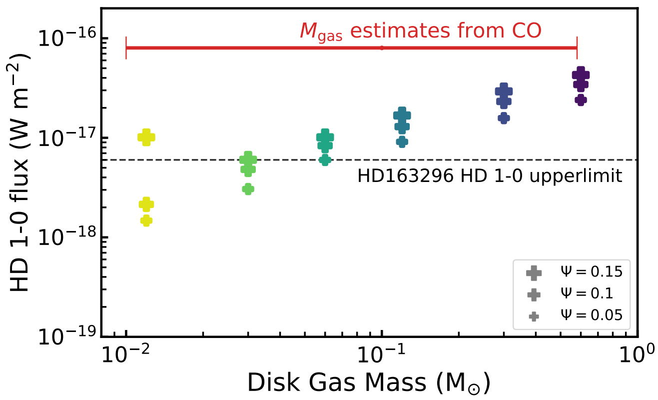

Fig. 5. Comparing the HD 163296 specific models to the HD 1–0 upper limit (Fedele et al. 2013). All models have a dust mass $M_{dust} = 6.6 \times 10^{-4}\ M_\odot$ (Table 3). The red bar shows the range of gas masses inferred from CO in the literature.

is that $\Delta_{g/d} \approx 20$–50. This relative depletion of gas over dust is supported by the hydrostatic MCMax modelling of the SED and low-J ^{12}CO, ^{13}CO, and C^{18}O lines by Boneberg et al. (2016), whose best models had $9.2 < \Delta_{g/d} < 18$. It is also consistent with the inner disc value $\Delta_{g/d} \approx 55$, measured using accretion onto the central star by Kama et al. (2015, their Fig. 2).

3. M_{gas} is far below our upper limit. In this hypothesis, the total C and O abundance in the gas must be enhanced above the interstellar baseline to still match the optically thin CO isotopologues. This would be the first known case of C and O enhancement, however the inner disc composition analysis by Kama et al. (2015) does not show evidence for a strong enhancement of gas-phase volatile elements over total hydrogen.

Thus $\Delta_{g/d} > 100$ is ruled out by the HD 1–0 upper limit for HD 163296, independently of assumptions about the precise abundance of gas-phase volatiles.

The abundance of volatile elements in the HD 163296 disc may be depleted or enhanced by up to a factor of a few, depending on the true value of M_{gas} and on the somewhat uncertain underlying number abundance ratios of ^{12}CO and its various isotopologues. We note that even with the flat, cold disc structure of HD 163296, our $\Delta_{g/d} = 100$ model somewhat over-predicts the CO emission outside of ∼100 au for an undepleted elemental carbon abundance (C/H $= 1.35 \times 10^{-4}$). A more flared surface would aggravate this over-prediction, while globally reducing the elemental C under-predicts the CO 3–2 inside ∼100 au. This may indicate that any depletion of gas-phase volatile elemental C and O, reflected in the CO abundance in the warm molecular layer, is restricted to the region beyond the CO snowline, which has been observed to be at ≈90 au (Qi et al. 2015). The same conclusion was recently reached by Zhang et al. (2019) through an analysis of spatially resolved C^{18}O data, which yielded a factor of ten depletion of gas-phase CO outside the CO snowline.

4.4. HD 100546

HD 100546 was previously modelled with `DALI` by Bruderer et al. (2012) who determined the radial and vertical structure of the disc mainly from CO lines and continuum emission. A refined version of this modelling effort included the *Herschel* HD upper limits, the C^0 and C$_2$H fluxes, and the spatially resolved CO 3–2 emission, constraining the gas mass to $8.1 \times 10^{-3} \leq M_{gas} \leq 2.4 \times 10^{-1}\ M_\odot$ (Kama et al. 2016). The highest mass model had $\Delta_{g/d} = 300$, with a dust mass anchored by the continuum spectral energy distribution. Owing to a factor of four error in the D abundance used in that model, we revise those numbers to ≲100 and thus $M_{gas} \lesssim 0.08\ M_\odot$ from the Kama et al. (2016) model. This is about a factor of two stronger than the constraint from our general model grid, so in Fig. 6 we adopt $M_{gas} \lesssim 0.08\ M_\odot$.

4.5. Other individual discs

HD 97048. Hosts a massive dust disc, $M_{dust} \simeq 6.7 \times 10^{-4}\ M_\odot$ (Walsh et al. 2016), so it is likely the gas mass is also high. The disc surface is highly flared ($\Psi = 0.5$–0.73; see e.g. Lagage et al. 2006; Walsh et al. 2016; Ginski et al. 2016; van der Plas et al. 2019). This exceeds the largest Ψ in our general grid, but we note again that the CO-surface Ψ and the density structure Ψ differ in physical meaning. From our grid we find $M_{gas} \leq 9.4 \times 10^{-2}\ M_\odot$ ($\Delta_{g/d} \leq 200$).

HD 104237. For this disc, Hales et al. (2014) determined $M_{dust} = 4 \times 10^{-4}\ M_\odot$, which assuming $\Delta_{g/d} = 100$ implies a total mass $M_{gas} = 4 \times 10^{-2}\ M_\odot$. This is consistent with our upper limit from HD 1–0, which yields an upper limit of $\Delta_{g/d} \leq 300$ (Fig. 2).

HD 36112 (MWC 758). Based on millimetre continuum interferometry, Guilloteau et al. (2011) inferred a disc mass of $(1.1 \pm 0.2) \times 10^{-2}\ M_\odot$. Our analysis of the 1.3 mm continuum flux and the HD 1 – 0 upper limit matches both data points for $\Delta_{g/d} \approx 100$ and a disc mass of order $10^{-2}\ M_\odot$. A substantially lower gas mass would imply a very low $\Delta_{g/d}$ mass ratio.

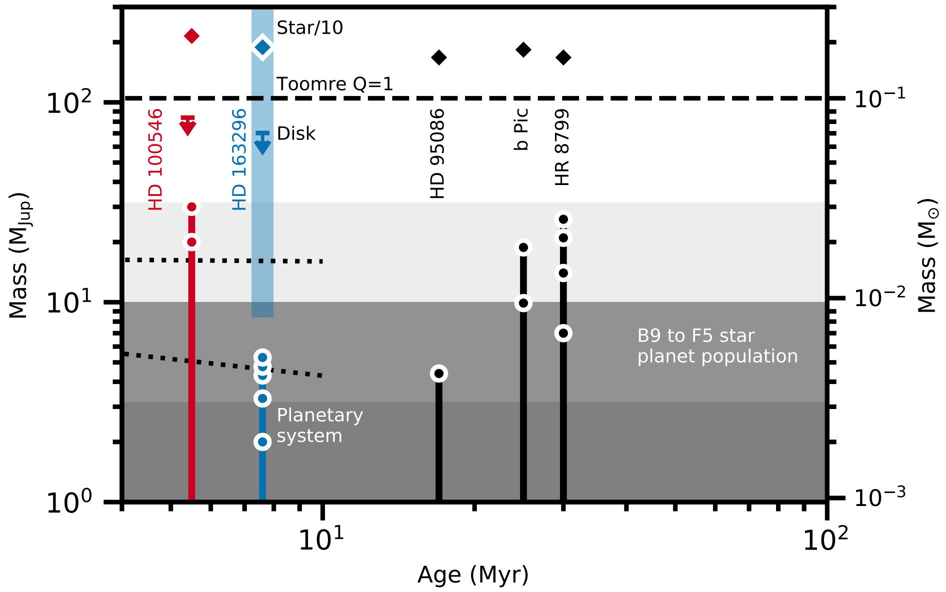

Fig. 6. Mass of selected discs and planets around B9 to F5 type stars. Vertical lines show the cumulative mass of each planetary system; dots highlight planets from the most massive at bottom. Disc gas mass upper limits from HD lines are taken from this work (HD 163296) and from Kama et al. (2016, HD 100546). For HD 163296, the range of CO isotopologue-based disc mass estimates is shown by a light blue bar (8×10^{-3} to $5.8 \times 10^{-1}\,M_\odot$; references in text). Also shown are the stellar mass divided by 10 and age; the mass limit for a gravitationally unstable disc (dashed line); an extrapolated dust-based disc mass range (dotted lines; Pascucci et al. 2016); and a population density colour map for planets around B9 to F5 type stars (data retrieved from `exoplanets.org` on 2019.07.16; bins contain from bottom to top 7, 6, and 1 planet). See text for individual planet and stellar mass references.

HD 31293 (AB Aurigae). From 1.3 mm continuum observations performed using the SMA, Andrews et al. (2013) inferred a dust mass of $(1.56 \pm 0.09) \times 10^{-4}\,M_\odot$, implying $M_{\rm gas} = 1.56 \times 10^{-2}\,M_\odot$ assuming $\Delta_{\rm g/d}$= 100. The high upper limit of HD 1–0 for this source does not allow us to put any meaningful constraints on the gas mass based on HD.

HD 135344B. It has been modelled by van der Marel et al. (2016) to determine the physical structure. Using ALMA observations of ^{13}CO $J = 3$–2, C^{18}O $J = 3$–2, ^{12}CO $J = 6$–5 and dust 690 GHz continuum, these authors determined a gas mass $M_{\rm gas} = 1.5 \times 10^{-2}\,M_\odot$. We ran models based on their physical structure and find the resulting HD 1–0 flux to be in agreement with the upper limit (see Fig. A.1).

HD 142527. Modelling interferometric 880 μm continuum and ^{13}CO 3–2 and C^{18}O 3–2 line observations, Boehler et al. (2017) determine a dust mass of $1.5 \times 10^{-3}\,M_\odot$ and a gas mass of $5.7 \times 10^{-3}\,M_\odot$ (see also Muto et al. 2015). This gives $3 \leq \Delta_{\rm g/d} \leq 5$ and suggests the gas is either strongly depleted in elemental C and O, or dissipating entirely. Because of the loose HD 1–0 upper limit for this source, we cannot provide an independent check of the low $\Delta_{\rm g/d}$ derived from CO.

HD 179218. From the integrated 1.3 mm flux Mannings & Sargent (2000) inferred a dust mass of $(1.5 \pm 0.15) \times 10^{-4}\,M_\odot$, implying $M_{\rm gas} = 1.5 \times 10^{-2}\,M_\odot$ assuming $\Delta_{\rm g/d} = 100$. Again the HD 1–0 upper limit provides no meaningful constraint on the gas mass.

HD 100453. Based on millimetre continuum interfermotric observations, van der Plas et al. (2019) infer a dust mass of $6.7 \times 10^{-5}\,M_\odot$. By comparing the ^{13}CO 2–1 and C^{18}O 2–1 to the disc model grid in Williams & Best (2014), they determine a gas mass of $(1 - 3\times) \times 10^{-3}\,M_\odot$. Combining both disc masses implies a gas-to-dust mass ratio of $\Delta_{\rm g/d}$ 15–45. From our analysis of the 1.3 mm continuum flux and the HD 1–0 upper limit we constrain gas mass to $M_{\rm gas} \leq 10^{-2}\,M_\odot$ and the gas-to-dust mass ratio $\Delta_{\rm g/d} \leq 300$. Both constraints are in agreement with the results of van der Plas et al. (2019).

HD 169142. From interferometric 1.3 mm continuum and ^{12}CO 2–1, ^{13}CO 2–1, and C^{18}O 2–1 line observations, Panić et al. (2008) derived a dust mass of $2.16 \times 10^{-4}\,M_\odot$ and a gas mass of $(0.6$–$3.0) \times 10^{-2}\,M_\odot$. Fedele et al. (2017) find similar disc masses based on higher resolution observations. Constraints based on our analysis of the 1.3 mm continuum flux and the HD 1–0 upper limit put the gas mass at $M_{\rm gas} \leq 4 \times 10^{-2}\,M_\odot$ and $\Delta_{\rm g/d} \leq 300$, both of which are in good agreement with previous results.

Oph IRS 48 (WLY 2-48). van der Marel et al. (2016) modelled the resolved 440 μm continuum and ^{13}CO 6–5 and C^{18}O 6–5 line observations. These authors derive a dust mass of $1.5 \times 10^{-5}\,M_\odot$ and a gas mass of $5.5 \times 10^{-4}\,M_\odot$, giving a gas-to-dust mass ratio of $\Delta_{\rm g/d} \approx 37$. Constraints from our analysis of the HD 1–0 line flux and 1.3 mm continuum give $M_{\rm gas} \lessapprox 10^{-2}\,M_\odot$ and $\Delta_{\rm g/d} \lessapprox 300$. These upper limits agree with previous results.

4.6. The gravitational stability of the discs

Constraints on $M_{\rm gas}$ allow us to test whether the discs in our sample are currently gravitationally stable. Gravitational instability, leading to spirals or fragmentation, occurs in disc regions which are dense and cold and have low orbital shearing on the timescale of the instability (i.e. at large radii). This is quantified with the Toomre Q parameter, $Q = \Omega_K\, c_{\rm s}\, (\pi\, G\, \Sigma)^{-1}$ (Toomre 1964), which simplifies to

$$Q = 21 \times \left(\frac{\Sigma}{10\,{\rm kg\,m^{-2}}}\right)^{-1} \times \left(\frac{r}{100\,{\rm au}}\right)^{-3/2}, \quad (3)$$

following Kimura & Tsuribe (2012). If $Q < 1$, the disc fragments. For $1 < Q < 2$, the disc is marginally stable, developing transient spirals and clumps, while for $Q > 2$ it is stable against gravitational collapse. Assuming a surface density profile $\Sigma = \Sigma_0 \times (r/r_0)^{-1}$ and $M_{\rm disc} \approx M_{\rm gas}$, we obtain

$$Q = 2.44 \times 10^{22}\, \pi\, r_0^{1/2}\, M_{\rm disc}^{-1}, \quad (4)$$

Our most massive disc models have $M_{\rm gas} = 0.1\,M_\odot$. Taking a characteristic radius $r_0 = 100$ au, we find $Q = 1.5$, which is marginally stable. The discs for which we have the weakest upper limits relative to the massive disc models – HD 142527, HD 144668, HD 179218, and HD 31293 – may potentially be gravitationally unstable within the limits of the

Herschel HD data. For the rest of the sample, a gravitationally unstable M_{gas} is effectively ruled out, i.e. they are most likely stable.

Dust dips, rings, or cavities may locally affect the temperature structure of the gas and thus, through the sound speed, the local Q in a disc ($Q \propto T_{kin}^{0.5}$, i.e. a weak dependence). In general, a lower dust surface density leads to more efficient external heating and thus more stability. Inside a local dust enhancement, the temperature may drop somewhat, but if the region is already very optically thick, the effect on T_{kin} is minor. We therefore have not considered the effect of such Σ_{dust} perturbations in this paper.

5. Discussion

5.1. Mass of discs, stars, and planets

Intermediate-mass stars (spectral types B9 to F5, masses 1.5–3 $M_{\odot}$) host some of the best-studied protoplanetary discs and high-mass planetary systems. Several Herbig Ae/Be protoplanetary discs have also yielded detections of protoplanet candidates. This presents an opportunity to investigate equivalent planetary systems at different stages of evolution.

In Fig. 6, we compare the disc gas mass with the host star and the candidate protoplanets in the disc. We show two Herbig Ae/Be systems with strong mass limits, HD 163296 ($M_{gas} \leq 0.067\ M_{\odot}$; this work) and HD 100546 ($M_{gas} \leq 0.08\ M_{\odot}$; Kama et al. 2016). Much of the work on embedded protoplanet candidates quoted below is very new. There are large, at least a factor of two to ten, uncertainties behind the planet mass estimates below, in particular for those inferred from dust gaps where the α viscosity parameter plays a role. We adopt middle-ground values from the literature to begin a discussion on comparing disc and embedded planet masses.

For HD 163296, our HD-based upper limit rules out a large fraction of the wide range of CO isotopologue based M_{gas} estimates from the literature. Of those still possible, the lowest is $M_{gas} = 8 \times 10^{-3}\ M_{\odot}$. The presence of five giant planets has been inferred from dust gaps and gas kinematics: at 10 au with a mass $(0.53 \pm 0.18)\ M_{Jup}$ for $\alpha_{visc} = 10^{-4}$ to 10^{-3} (Zhang et al. 2018); at 48 au with 0.46 M_{Jup} (Isella et al. 2016; Liu et al. 2018); at 86 au with $(1 \pm 0.5)\ M_{Jup}$ (Liu et al. 2018; Teague et al. 2018); at 145 au with 1.3 M_{Jup} (Liu et al. 2018; Teague et al. 2018); and at 260 au with 2 M_{Jup} (Pinte et al. 2018). Using the HD- and CO-based M_{gas} limits, and taking the combined mass of all published protoplanets in this disc as $\approx 5\ M_{Jup}$, we find the HD 163296 disc has converted 10–40% of its mass into giant planets.

For HD 100546, the planet masses were constrained to be $\approx 10\ M_{Jup}$ at 10 au and $\sim 10\ M_{Jup}$ at 70 au by Pinilla et al. (2015). The mass of the outer planet could be $<5\ M_{Jup}$ ($>15\ M_{Jup}$) if it formed very early (late), so we adopt 10 M_{Jup}. The HD-based M_{gas} upper limit and the combined mass of the candidate planets yield a lower limit on the disc-to-planet mass conversion efficiency of $\gtrsim 30\%$.

Such high disc-to-planet mass conversion efficiencies combined with the presence of several gas giants per star raise the question of whether the planets formed through gravitational instability. Adding the M_{gas} upper limit and combined mass of proposed planets in either disc gives a result close to 0.1 $M_{\odot}$. This is approximately at the gravitationally unstable limit, so such a formation pathway may be feasible even with the current total mass in the system, although the local Toomre Q varies with radius and may leave the outer disc still far from instability (e.g. Booth et al. 2019).

We also show in Fig. 6 three somewhat older stars of similar mass (HD 95086, β Pic, and HR 8799) and their planets; standard disc mass estimates for stars of 1.5 and 3 $M_{\odot}$ based on M_{dust} relations from Pascucci et al. (2016) and scaled up with $\Delta_{g/d} = 100$; and a shaded log-scale histogram of the mass distribution of known planets around early-type stars[1]. Stellar masses are from the *Gaia* DR2 analysis by Vioque et al. (2018), and from David & Hillenbrand (2015, β Pic) and Stassun et al. (2018, HD 95086). Planet masses for individual systems are plotted as cumulative bars with the highest mass planet at the base. We compiled planet data from Teague et al. (2018), Pinte et al. (2018, 2019), Pinilla et al. (2015), Liu et al. (2018), Zhang et al. (2018), Rameau et al. (2013a,b), De Rosa et al. (2016), and Marois et al. (2008, 2010). Individual stellar masses are from Rhee et al. (2007), David & Hillenbrand (2015), Stassun et al. (2018), and Vioque et al. (2018).

The two HD-based disc M_{gas} limits in Fig. 6 exceed the combined mass of planets around HR 8799, the most massive known planetary system, by a factor of only three. The disc mass limits are also only a factor of three above combined mass of candidate protoplanets in the HD 100546 disc. Either A-type star discs can, in some cases, convert 10% or more of their mass into giant planets, or these planetary systems formed at a very early stage, perhaps while the central protostar and massive initial disc were still heavily accreting from the protostellar envelope in which they were embedded. The mass distribution of giant planets around main-sequence A and B stars (Fig. 6) is strongly skewed towards lower masses, suggesting that such extreme mass conversion events are either rare, or that the high-mass planetary systems are not stable on timescales beyond a few times 10 Myr.

5.2. Observing HD in Herbig discs with SOFIA/HIRMES, SPICA/SAFARI and Origins Space Telescope

In the coming years, several facilities will or may become available for observing HD rotational lines. The HIRMES instrument for SOFIA is currently undergoing commissioning and is due to be delivered at the end of 2020 (Richards et al. 2018). HIRMES will have a high spectral resolution of $R \sim 100\,000$, allowing us for the first time to spectrally resolve the HD 1–0 line. The sensitivity of HIRMES will be similar to Herschel/PACS. Our models suggest some Herbig Ae/Be discs will be detectable with this instrument, assuming the necessary hours per source are available.

Figure 7 shows the detectability of our disc models with a 10 h SOFIA/HIRMES observation, assuming a distance of 150 pc. Of the flat models (group II discs), only the most massive ($M_{gas} \sim 0.1\ M_{\odot}$) around stars with the highest stellar luminosity ($L_{*} \geq 50\ L_{\odot}$) are detectable. Among the flared models (group I), a larger fraction of discs is observable. All of the disc models $M_{gas} = 0.1\ M_{\odot}$ where $\Delta_{gd} > 10$ should be detectable in 10 h with SOFIA/HIRMES. For those discs with $M_{gas} = 0.01\ M_{\odot}$, all systems with $L_{*} = 125\ L_{\odot}$ and most systems with $L_{*} = 50\ L_{\odot}$ are detectable. To maximise the chance of success, future SOFIA/HIRMES observations should select group I sources with high stellar luminosity.

Based on the stellar luminosities in Table 1 there are four group I sources that match these criteria best for SOFIA/HIRMES to detect the HD 1–0 line: HD 31293 (AB Aur), HD 100546, HD 179218 and HD 97048. For these sources a 10 h observation with SOFIA/HIRMES would improve the current upper limits by a factor 3–10 and constrain the gas-to-dust mass ratio to $\Delta_{g/d} \leq 50-100$ if the sources remain undetected.

[1] Planets retrieved from `exoplanets.org` on 2019.07.16.

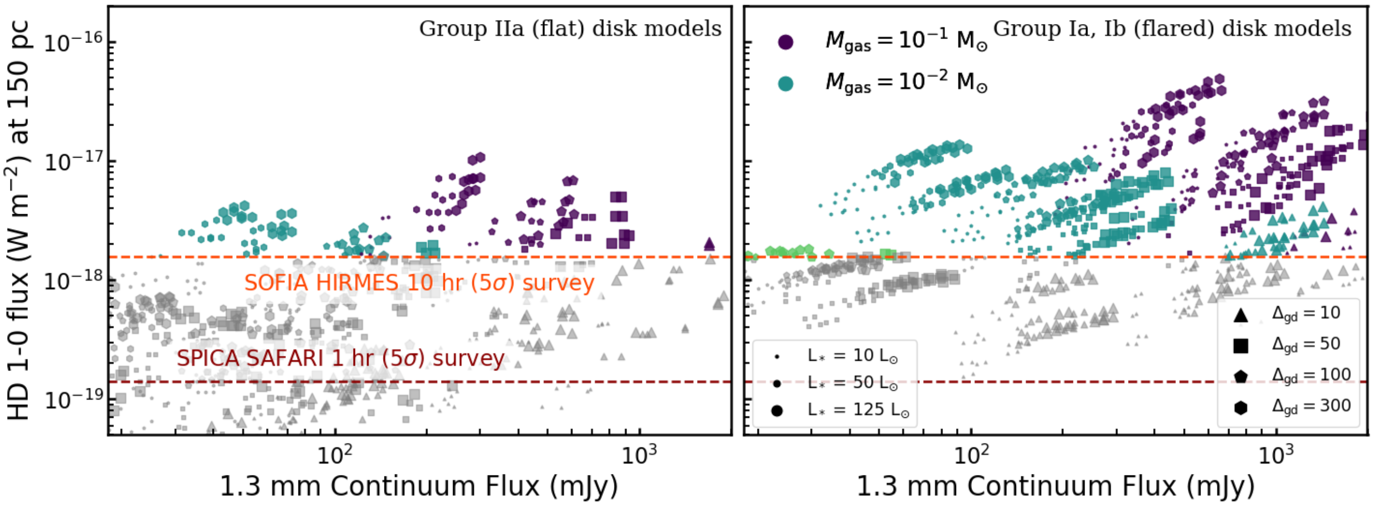

Fig. 7. Observability of Group Ia,Ib (*left*) and Group IIa (*right*) models with SOFIA HIRMES. Coloured disc models are detectable ($\geq 5\sigma$) with a 10 h integration. Dark red dashed line shows the SPICA/SAFARI 1 h detection limit. The Origins Space Telescope 1 h detection limit ($\sim 1 \times 10^{-20}$ W m^{-2}) lies below the limits of the figure. The fluxes are calculated for a distance of 150 pc.

Beyond SOFIA/HIRMES there are two proposed space missions focussing on far-infrared observations: SPICA/SAFARI and Origins Space Telescope. The SPICA mission is one of the competitors for ESA's M5 opportunity, with a resolving power $R \sim 3000$ and a 5σ 1 h sensitivity of 1.3×10^{-19} W m^{-2} at 112 μm (Audley et al. 2018). The Origin Space Telescope is a NASA mission concept. It would have high spectral resolution ($R \sim 43\,000$) and sensitivity ($\sim 1 \times 10^{-20}$ W m^{-2} in 1 h) at 112 μm (Bonato et al. 2019). Hydrogen deuteride in all Herbig Ae/Be discs, and many T Tauri discs, within $\sim$200 pc will be detectable with these missions. However, both still require final approval and would only become available at the end of the 2020 s at the earliest. If approved, these missions would be an enormous step forward in planet-forming disc studies.

6. Conclusions

We have studied the significance, in terms of total gas mass, of *Herschel* Space Observatory upper limits on HD 1–0 line emission for 15 individual protoplanetary discs. We find an overall gas mass upper limit of $M_{gas} \leq 0.1\,M_{\odot}$ for most of the discs studied. None of the discs are very likely to be strongly gravitationally unstable, although the constraints for HD 142527, HD 144668, HD 179218, and HD 31293 (AB Aur) are weak enough to allow for the possibility.

The HD 163296 disc mass is $M_{gas} \leq 6.7 \times 10^{-2}\,M_{\odot}$, based on the HD 1–0 upper limit. The CO-based literature lower limit is $M_{gas} = 8 \times 10^{-3}\,M_{\odot}$, which is contingent on the true level of gas-phase volatile depletion. The gas-to-dust ratio is thus $12 \leq \Delta_{g/d} \leq 100$, indicating gas dissipation may be proceeding faster than dust removal in this disc. This is consistent with $\Delta_{g/d} = 55$ inferred from the accretion-contaminated photosphere of the central star (Kama et al. 2015).

Comparing the HD 163296 and HD 100546 M_{gas} constraints with their protoplanet candidates and the HR 8799 giant planet system, we find that at least some Herbig Ae/Be discs convert the equivalent of 10–40% of their present-day mass into giant planets.

Near-future SOFIA/HIRMES observations will probe the mass of flaring discs and large flat discs around A-type stars within $\approx$150 pc with $\gtrsim$10 h integrations. The SPICA/SAFARI mission will be crucial for larger sample studies of M_{gas} in discs. The Origins Space Telescope, if approved, would further revolutionise the field.

Acknowledgements. We thank Sebastiaan Krijt for useful discussions. M.K. gratefully acknowledges funding from the European Union's Horizon 2020 research and innovation programme under the Marie Sklodowska-Curie Fellowship grant agreement No 753799. L.T. is supported by NWO grant 614.001.352. D.F. acknowledges financial support provided by the Italian Ministry of Education, Universities and Research, project SIR (RBSI14ZRHR). A.M. and C.C. gratefully acknowledge funding from the European Union's Horizon 2020 research and innovation programme under the Marie Sklodowska-Curie grant agreement No 823823, (RISE DUSTBUSTERS), and A.M. funding by the Deutsche Forschungsgemeinschaft (DFG, German Research Foundation) – Ref no. FOR2634/1 ER685/11-1. E.A.B. gratefully acknowledges support from NASA via grant NNX16AB48G-XRP. All figures were generated with the PYTHON-based package MATPLOTLIB (Hunter 2007).

References

Andrews, S. M., Rosenfeld, K. A., Kraus, A. L., & Wilner, D. J. 2013, ApJ, 771, 129
Audley, M. D., de Lange, G., Gao, J.-R., et al. 2018, SPIE Conf. Ser., 10708, 107080K
Bergin, E. A., Cleeves, L. I., Gorti, U., et al. 2013, Nature, 493, 644
Boehler, Y., Weaver, E., Isella, A., et al. 2017, ApJ, 840, 60
Bonato, M., De Zotti, G., Leisawitz, D., et al. 2019, PASA, 36, e017
Boneberg, D. M., Panić, O., Haworth, T. J., Clarke, C. J., & Min, M. 2016, MNRAS, 461, 385
Booth, A. S., Walsh, C., Ilee, J. D., et al. 2019, ApJL, 882, L31
Brown, A., Vallenari, A., Prusti, T., et al. 2018, A&A, 616, A1
Bruderer, S. 2013, A&A, 559, A46
Bruderer, S., van Dishoeck, E. F., Doty, S. D., & Herczeg, G. J. 2012, A&A, 541, A91
David, T. J., & Hillenbrand, L. A. 2015, ApJ, 804, 146
de Gregorio-Monsalvo, I., Ménard, F., Dent, W., et al. 2013, A&A, 557, A133
De Rosa, R. J., Rameau, J., Patience, J., et al. 2016, ApJ, 824, 121
Ellerbroek, L. E., Benisty, M., Kraus, S., et al. 2015, A&A, 573, A77
Fairlamb, J. R., Oudmaijer, R. D., Mendigutía, I., Ilee, J. D., & van den Ancker, M. E. 2015, MNRAS, 453, 976
Favre, C., Cleeves, L. I., Bergin, E. A., Qi, C., & Blake, G. A. 2013, ApJ, 776, L38
Fedele, D., Bruderer, S., van Dishoeck, E. F., et al. 2013, A&A, 559, A77
Fedele, D., Carney, M., Hogerheijde, M. R., et al. 2017, A&A, 600, A72
Folsom, C. P., Bagnulo, S., Wade, G. A., et al. 2012, MNRAS, 422, 2072
Ginski, C., Stolker, T., Pinilla, P., et al. 2016, A&A, 595, A112
Guilloteau, S., Dutrey, A., Piétu, V., & Boehler, Y. 2011, A&A, 529, A105
Hales, A. S., De Gregorio-Monsalvo, I., Montesinos, B., et al. 2014, AJ, 148, 47

Hartmann, L., Calvet, N., Gullbring, E., & D'Alessio, P. 1998, ApJ, 495, 385
Hunter, J. D. 2007, Comput. Sci. Eng., 9, 90
Isella, A., Testi, L., Natta, A., et al. 2007, A&A, 469, 213
Isella, A., Guidi, G., Testi, L., et al. 2016, Phys. Rev. Lett., 117, 251101
Kama, M., Folsom, C. P., & Pinilla, P. 2015, A&A, 582, L10
Kama, M., Bruderer, S., Carney, M., et al. 2016, A&A, 588, A108
Kenyon, S. J., & Hartmann, L. 1987, ApJ, 323, 714
Kimura, S. S., & Tsuribe, T. 2012, PASJ, 64, 116
Lagage, P.-O., Doucet, C., Pantin, E., et al. 2006, Science, 314, 621
Liu, S.-F., Jin, S., Li, S., Isella, A., & Li, H. 2018, ApJ, 857, 87
Lodders, K. 2003, ApJ, 591, 1220
Lynden-Bell, D., & Pringle, J. E. 1974, MNRAS, 168, 603
Maaskant, K. M., Honda, M., Waters, L. B. F. M., et al. 2013, A&A, 555, A64
Maaskant, K. M., Min, M., Waters, L. B. F. M., & Tielens, A. G. G. M. 2014, A&A, 563, A78
Mannings, V., & Sargent, A. I. 2000, ApJ, 529, 391
Marois, C., Macintosh, B., Barman, T., et al. 2008, Science, 322, 1348
Marois, C., Zuckerman, B., Konopacky, Q. M., Macintosh, B., & Barman, T. 2010, Nature, 468, 1080
McClure, M. K., Bergin, E. A., Cleeves, L. I., et al. 2016, ApJ, 831, 167
Meeus, G., Waters, L. B. F. M., Bouwman, J., et al. 2001, A&A, 365, 476
Meeus, G., Salyk, C., Bruderer, S., et al. 2013, A&A, 559, A84
Miotello, A., van Dishoeck, E. F., Kama, M., & Bruderer, S. 2016, A&A, 594, A85
Muto, T., Tsukagoshi, T., Momose, M., et al. 2015, PASJ, 67, 122
Nakagawa, T., Shibai, H., Onaka, T., et al. 2014, SPIE, 9143, 91431I
Panić, O., Hogerheijde, M. R., Wilner, D., & Qi, C. 2008, A&A, 491, 219
Pascucci, I., Testi, L., Herczeg, G. J., et al. 2016, ApJ, 831, 125
Pilbratt, G. L., Riedinger, J. R., Passvogel, T., et al. 2010, A&A, 518, L1
Pinilla, P., Birnstiel, T., & Walsh, C. 2015, A&A, 580, A105
Pinte, C., Price, D., Ménard, F., et al. 2018, ApJ, 860, L13
Pinte, C., van der Plas, G., Menard, F., et al. 2019, Nat. Astron., 3, 1109
Poglitsch, A., Waelkens, C., Geis, N., et al. 2010, A&A, 518, L2
Powell, D., Murray-Clay, R., Pérez, L. M., Schlichting, H. E., & Rosenthal, M. 2019, ApJ, 878, 116
Prodanović, T., Steigman, G., & Fields, B. D. 2010, MNRAS, 406, 1108
Qi, C., Öberg, K. I., Andrews, S. M., et al. 2015, ApJ, 813, 128
Rameau, J., Chauvin, G., Lagrange, A. M., et al. 2013a, ApJ, 772, L15
Rameau, J., Chauvin, G., Lagrange, A. M., et al. 2013b, ApJ, 779, L26
Rhee, J. H., Song, I., Zuckerman, B., & McElwain, M. 2007, ApJ, 660, 1556
Richards, S. N., Moseley, S. H., Stacey, G., et al. 2018, J. Astron. Instrum., 7, 1840015
Rosenfeld, K. A., Andrews, S. M., Hughes, A. M., Wilner, D. J., & Qi, C. 2013, ApJ, 774, 16
Salyk, C., Herczeg, G. J., Brown, J. M., et al. 2013, ApJ, 769, 21
Stassun, K. G., Oelkers, R. J., Pepper, J., et al. 2018, AJ, 156, 102
Teague, R., Bae, J., Bergin, E. A., Birnstiel, T., & Foreman-Mackey, D. 2018, ApJ, 860, L12
Tilling, I., Woitke, P., Meeus, G., et al. 2012, A&A, 538, A20
Toomre, A. 1964, ApJ, 139, 1217
Trapman, L., Miotello, A., Kama, M., van Dishoeck, E. F., & Bruderer, S. 2017, A&A, 605, A69
van der Marel, N., van Dishoeck, E. F., Bruderer, S., Pérez, L., & Isella, A. 2015, A&A, 579, A106
van der Marel, N., van Dishoeck, E. F., Bruderer, S., et al. 2016, A&A, 585, A58
van der Plas, G., Ménard, F., Gonzalez, J. F., et al. 2019, A&A, 624, A33
Vioque, M., Oudmaijer, R. D., Baines, D., Mendigutía, I., & Pérez-Martínez, R. 2018, A&A, 620, A128
Walsh, C., Juhász, A., Meeus, G., et al. 2016, ApJ, 831, 200
Weingartner, J. C., & Draine, B. T. 2001, ApJ, 548, 296
Williams, J. P., & Best, W. M. J. 2014, ApJ, 788, 59
Williams, J. P., & McPartland, C. 2016, ApJ, 830, 32
Woitke, P., Kamp, I., Antonellini, S., et al. 2019, PASP, 131, 064301
Woodall, J., Agúndez, M., Markwick-Kemper, A. J., & Millar, T. J. 2007, A&A, 466, 1197
Zhang, S., Zhu, Z., Huang, J., et al. 2018, ApJ, 869, L47
Zhang, K., Bergin, E. A., Schwarz, K., Krijt, S., & Ciesla, F. 2019, ApJ, 883, 98

Appendix A: HD 1–0 fluxes for HD 135344B

Based on the HD 135344B source-specific model from van der Marel et al. (2015, 2016), we ran a series of ten models, varying the disc gas mass between $3.75\times10^{-3}\ M_\odot$ and $3\times10^{-2}\ M_\odot$. Figure A.1 compares the HD 1–0 line fluxes of these models to the observed upper limit (Table 1). From the CO isotopologue observations van der Marel et al. (2016) infer $M_{\rm gas} = 1.5\times10^{-2}\ M_\odot$. This gas mass is in agreement with the gas mass upper limit inferred from HD 1–0, $M_{\rm gas} \leq 2.3\times10^{-2}\ M_\odot$. We note that both gas masses are much lower than $0.1\ M_\odot$, making it highly unlikely that HD 135344B is gravitationally unstable (Sect. 4.6).

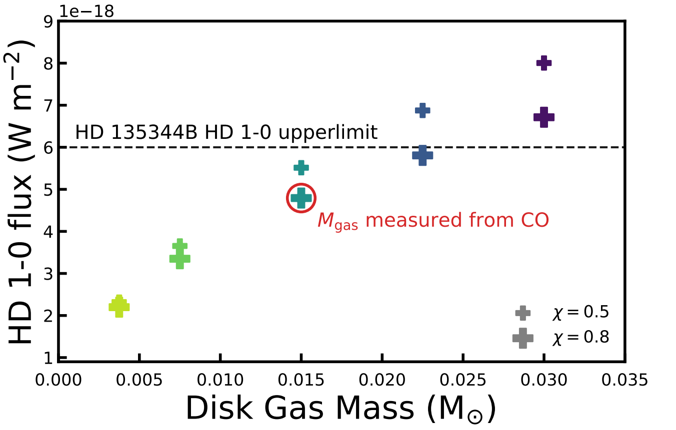

Fig. A.1. Comparing the HD 135344B specific models from van der Marel et al. (2016) to HD 1–0 upper limit (Fedele et al. 2013). All models have a dust mass $M_{\rm dust} = 1.3\times10^{-4}\ M_\odot$ (cf. Table 3 in van der Marel et al. 2016). The red circle shows the gas mass inferred from CO by van der Marel et al. (2016).

Appendix B: HD 2–1 upper limits versus the model fluxes

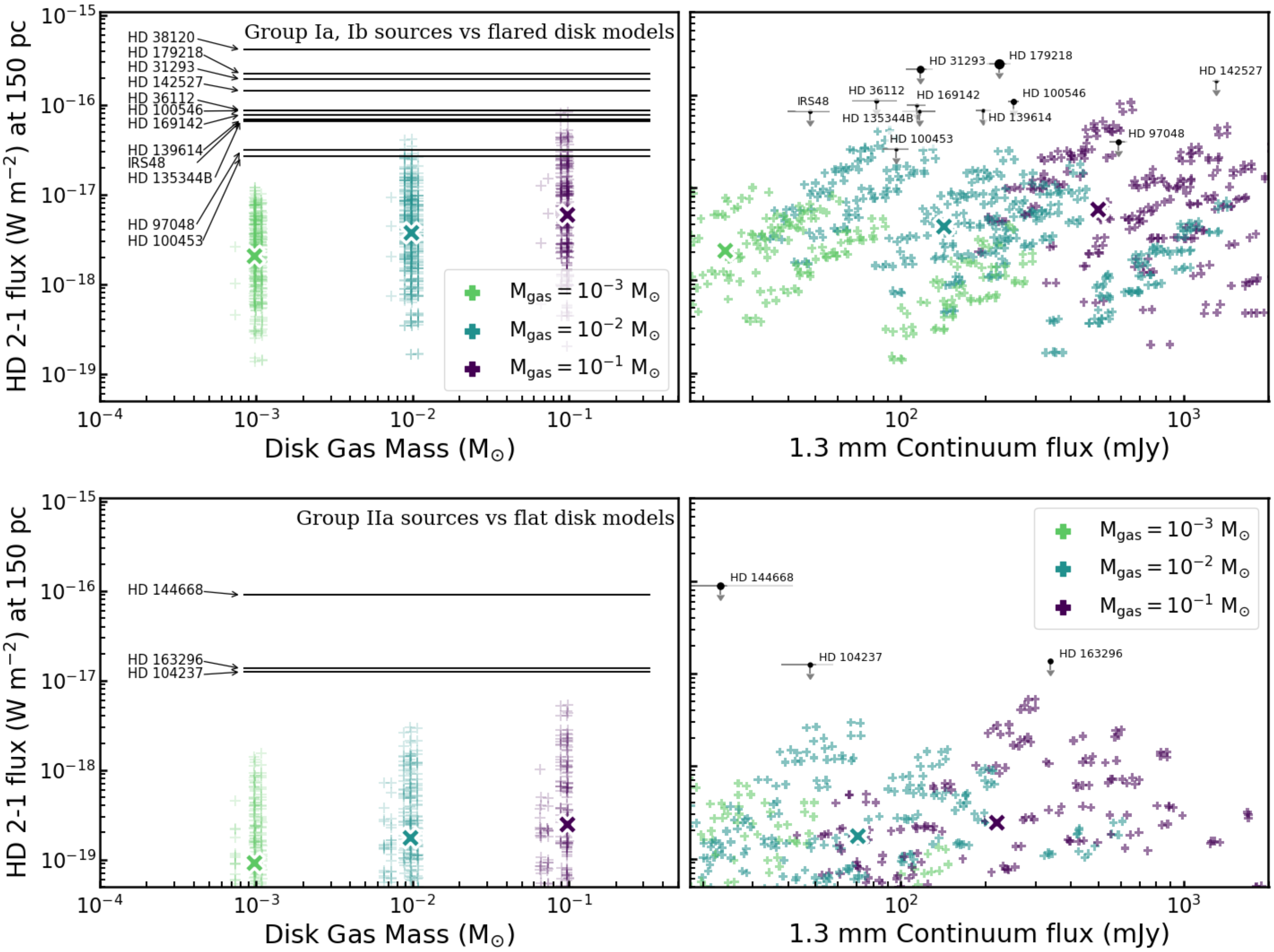

Fig. B.1. Upper limits on HD 56 μm line flux for the sample of Herbig Ae/Be disc systems (black lines) compared with our grid of `DALI` disc models (crosses). The top panels show the group I sources compared to models with flaring angle $\psi = 0.3$. The bottom panels show the group II sources compared to models with $\psi = 0.0$. *Left*: models are separated based on gas mass. *Right*: HD 2–1 upper limits set against 1.3 mm continuum fluxes for both observations and models.

Appendix C: HD 1–0 line versus 1.3 mm continuum fluxes, showing gas-to-dust ratios and stellar luminosities

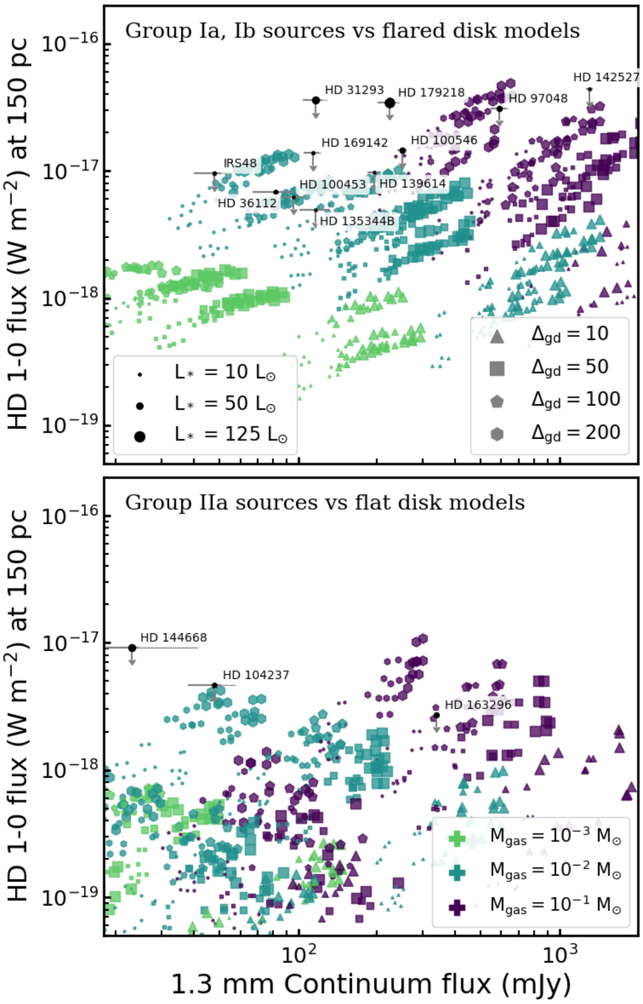

Fig. C.1. HD 1–0 line flux vs. 1.3 mm continuum fluxes for both observations and models. The panels are similar to right panels of Fig. 2, but also show the model gas-to-dust mass ratios (marker shape) and stellar luminosities (marker size).